[Technical Note]

Comparison of edge enhancements by phase contrast imaging and post-processing with unsharp masking or Laplacian filtering

Satoru MATSUO[†], Junji MORISHITA[††], Tetsuro KATAFUCHI[†††], and Hiroshi FUJITA[††††]

[†]Department of Radiological Technology, Faculty of Medical Science, Kyoto College of Medical Science,
1-3 Imakita, Oyamada-higashi, Sonobe, Nantan, Kyoto, Japan 622-0044
[††]Department of Health Sciences, Faculty of Medical Sciences, Kyushu University,
3-1-1 Maidashi, Higashi-ku, Fukuoka, Fukuoka, Japan 812-8582
[†††]Department of Radiological Technology, School of Health Science, Gifu University of Medical Science,
795-1 Nagamine Ichihiraga, Seki, Gifu, Japan 501-3892
[††††]Department of Intelligent Image Information, Graduate School of Medicine, Gifu University,
1-1 Yanagido, Gifu, Gifu, Japan 501-1194
(Received on July 23, 2016. In final form on September 23, 2016)

Abstract : Digital phase-contrast-imaging (phase-imaging) using a small-focus X-ray tube provides images with greater sharpness than conventional X-ray imaging (conventional-imaging), because the phase-imaging can produce images that are edge-enhanced at the boundary of an object because of refracted X-rays. In the present study, by performing image processing on a conventional-image we investigated whether we can produce an edge-enhanced conventional-image of equal edge-enhancement effect to that of phase-imaging. We used unsharp masking and Laplacian filtering as post-processing for edge enhancement of conventional-images. To determine the image processing parameters, the profile curves of acrylic fibers were used. Using these optimal imaging parameters, image processing was done on conventional-images of acrylic phantoms, followed by image quality comparisons of the post-processed conventional-images (post-processed-images) and phase-images. Furthermore, we performed a frequency analysis of the phase-image, conventional-image, and post-processed-image. Edge-enhanced conventional-images were obtained with a similar but slightly lower edge-enhancement effect than phase-images by processing images with appropriate parameters for unsharp masking and for Laplacian filtering. However, an increase in noise occurred because of the edge-enhancement processing. Edge-enhanced conventional-images of similar edge-enhancement effect to phase-images are obtainable by image processing of conventional-images. However, the edge clarity of the post-processed-images is somewhat worse than that of phase-images. Moreover, the edge-enhancement effect of post-processed-images is far lower than that of phase-images, because of increased noise resulting from the image processing.
Keywords : phase-contrast-imaging, edge-enhancement, unsharp masking, Laplacian filtering, image quality

1. INTRODUCTION

When X-rays pass through an object, refraction and interference occur because of the nature of electromagnetic waves. The difference in X-ray absorption caused by refraction and interference is called "phase contrast," and using this, edge-enhanced images can be obtained. In the 1990s, the X-ray phase-contrast technique was developed using special X-ray sources, such as synchrotron radiation or microfocus X-ray tubes [1-6]. In the 2000s, several papers reported on phase-contrast imaging (herein referred to as phase imaging) using a small-focus X-ray tube [7-14]. Based on the theory of Wilkins [3], Kotre et al. investigated phase imaging using a conventional X-ray tube in mammography [7]. To obtain high coherence, the object was placed 2.0 m or more away from the X-ray tube in their experimental study. Wu et al. theoretically investigated phase-contrast mammography with coherent X-rays from an X-ray tube with a focal spot of 0.025 mm [10]. Fitzgerald reviewed the phase imaging techniques and concluded that the phase-contrast technique is useful for mammography [5]. However, the high degree of coherence required for phase imaging in the techniques cited above is an obstacle to the clinical use of phase-contrast techniques. Ishisaka et al. presented a new method of analyzing the edge effect in phase imaging with incoherent X-rays [8]. Honda et al. reported on phase-contrast mammography using a practical molybdenum anode tube and mammography screen-film system based on the theoretical method [9]. In these studies, the fundamentals of phase-contrast techniques were established for clinical mammography.

Especially in particular, in clinical mammography the development of a high-resolution system was necessary in order to improve our ability to detect micro calcifications.

Figure 1 is a diagram of a phase-imaging configuration with a small-focus X-ray tube. Conventional X-ray images are made using the attenuation of the radiation due to absorption of X-rays when they pass through an object [Fig.1(a)]. Phase imaging provides edge-enhancement in the periphery of an object due to refraction of X-rays. In other words, the X-ray intensity on an X-ray detector after the X-rays pass through an object becomes more intense in the area outside of an object but less intense inside of the imaged object because of the refracted X-rays, thereby enhancing the edge [Fig.1(b)]. This phenomenon is not seen in conventional X-ray imaging (herein referred to as conventional imaging), as the displacement due to X-ray refraction is negligibly small. In phase imaging, a sufficient distance is necessary between the detector and the object to obtain a noticeable edge-enhancement effect using the

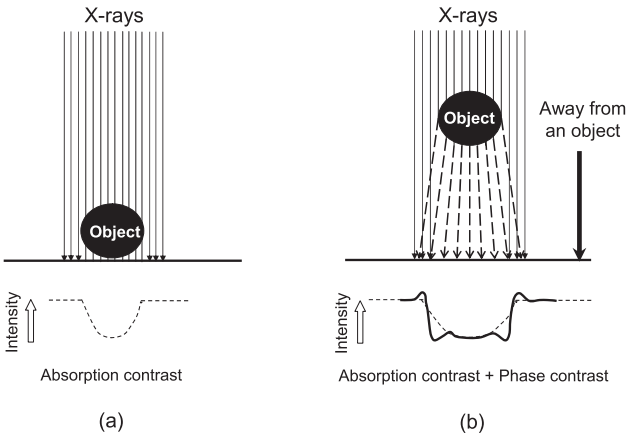

Fig.1 Schematic diagram of phase contrast imaging configuration with a small-focus X-ray tube.
(a) Conventional imaging and (b) phase contrast imaging. The edge-enhancement effect results from a superposition of the phase contrast on an absorption contrast image. Note that the detector (image plane) should be a distance away from the object for phase contrast imaging.

subtle refraction of X-rays [3-10]. Magnified phase imaging with a small-focus X-ray tube is based on such a method.

An intensifying screen/film system was used for X-ray detection in a phase imaging system, which allowed both an improvement in image sharpness due to edge-enhancement effects using refracted X-rays and an improvement in image resolution due to the rescaling effect [15]. However, problems such as an increased radiation dose and image magnification remained when phase imaging (i.e., "analog" type imaging) was performed using a screen/film system. Therefore, photostimulable phosphor ("imaging") plates for a highly sensitive phase imaging mammography system were developed, along with digital phase imaging using computed radiography (CR), enabling reductions of image size and noise [15, 16]. A digital phase-contrast mammography (PCM) system [17-24] utilizing this technology was manufactured in 2005 and has been used in clinical practice mainly in Japan.

Interestingly, Donnelly, et al. reported that phase components, which are extracted from phase images by dual focal-spot imaging, contain an edge-enhancement effect similar to that of unsharp masking, a standard tool in image processing [12]. Thus, one may naturally surmise that images edge-enhanced by unsharp masking on digital images obtained by conventional imaging may be obtainable as an alternative to PCM. If edge-enhanced images with a quality equivalent to that of PCM could be obtained with image processing of conventional images (herein referred to as post-processed images), such image processing methods could help reduce expenses by replacing expensive specialized equipment.

The aim of our study is to investigate whether the image processing method can be an alternative to the phase imaging method by comparing the edge-enhancement effect obtained by both methods. First, the edge-enhancement effect of phase imaging was analyzed using acrylic fibers. Second, using profile curves of acrylic fibers imaged by conventional imaging, the image processing parameters necessary to obtain an edge enhancement equivalent to that of phase imaging were determined. In this way, post-processed images with optimal image processing parameters and phase images were visually evaluated. Also, frequency analyses were performed.

2. Theory of the image processing method to improve sharpness

For improvement of image sharpness, we used unsharp masking, which has been generally used for medical imaging, and Laplacian filtering, which has been generally used in the engineering field [25,26].

2.1 Unsharp masking

There are three steps to improve sharpness by unsharp masking. The first step is to form a blurred image, which can be obtained by smoothing a raw image. The second step is to form a subtraction image, which is obtained by subtracting the blurred image from the raw image. Thus, the subtraction image is formed by extracting the high-frequency components from the raw image. The third step is to form a processed image, which can be obtained by adding a weighted subtraction image to the raw image. Unsharp masking performed in the real-space domain is expressed by the following [25] :

$$G(x,y) = f(x,y) + k\{f(x,y) - f_u(x,y)\}, \quad (1)$$

$$f_u(x,y) = \frac{1}{m \times n} \sum_{j=1}^{m} \sum_{i=1}^{n} f(x_i, y_j), \quad (2)$$

$f(x,y)$ and $G(x,y)$ show a raw image and a processed image, respectively, and $f_u(x,y)$ in Eq.(2) shows the mean value of the $m \times n$ pixels (m and n are integers) centered on the coordinates (x,y) of the raw image. The enhanced spatial frequency range depends on the size of the mask (herein referred to as "mask size"), namely, $m \times n$, and the degree of enhancement is determined by the weighting factor k (a real number).

2.2 Laplacian filtering

Sharpening by Laplacian filtering involves two steps. The first step is the formation of edge-enhanced images, which can be obtained using the second partial derivatives of a raw image. The second step is the formation of a processed image, which can be obtained by subtracting the edge-enhanced image from the raw image. Laplacian filtering performed in the real-space domain is expressed by the following :

$$G(x,y) = f(x,y) + k\nabla^2 f(x,y), \quad (3)$$

where $f(x,y)$ and $G(x,y)$ show a raw image and a processed image, respectively, $\nabla^2 f$ is the Laplacian of $f(x,y)$, and the degree of enhancement is determined by the weighting factor k (a real number). The Laplacian $\nabla^2 f$ is defined as the sum of the second partial derivative $\Delta^2 x$ with respect to x and the second partial derivative $\Delta^2 y$ with respect to y of a 2D image $f(x,y)$, which is expressed as the following [25] :

$$\nabla^2 f(x,y) = \frac{\partial^2 f(x,y)}{\partial x^2} + \frac{\partial^2 f(x,y)}{\partial y^2} \equiv \Delta^2 x + \Delta^2 y. \quad (4)$$

When the mask size is 3×3, the second derivatives $\Delta^2 x$ and $\Delta^2 y$ in the x and y directions are expressed in Eqs.(5) and (6), respectively, and thus, the Laplacian $\nabla^2 f$ is expressed in Eq.(7) as follows.

$$\Delta^2 x = (f(x-1,y) - f(x,y)) - (f(x,y) - f(x+1,y)). \quad (5)$$

$$\Delta^2 y = (f(x,y-1) - f(x,y)) - (f(x,y) - f(x,y+1)). \quad (6)$$

$$\nabla^2 f(x,y) = f(x+1,y) + f(x-1,y) + f(x,y+1) + f(x,y-1) - 4f(x,y). \quad (7)$$

3. MATERIALS AND METHODS

3.1 PCM system

The PCM system consisted of a mammography unit, a CR (Mermaid, Konica Minolta, Tokyo, Japan) unit, and a dry laser printer, as shown in Fig.2. Conventional mammography producing contact images and PCM producing 1.75 times magnified images could be performed with the PCM system [19, 20]. The nominal focal-spot sizes for conventional mammography and PCM were 0.3 mm and 0.1 mm, respectively. The distance between the focal spot of the X-ray tube and the object was 650mm. In conventional mammography, the detector (photostimulable phosphor plate: RP-6M, Konica Minolta, Tokyo, Japan) was positioned directly behind the object with a bucky [Fig.2(a)], whereas in PCM, the detector was positioned 490 mm away from the object without a bucky [Fig.2(b)].

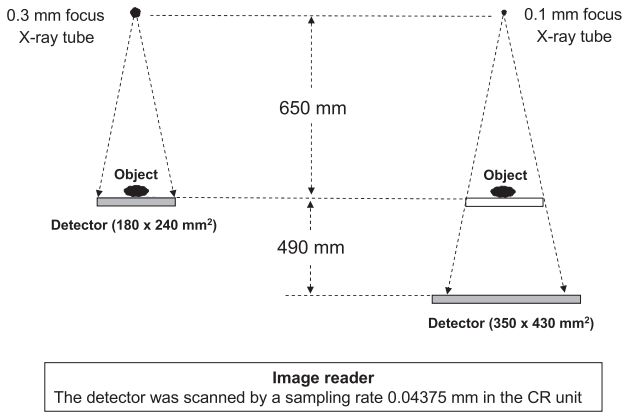

Fig.2 Schematic diagram of digital phase contrast mammography (right) and conventional imaging (left).

The size of the photostimulable phosphor plate for conventional mammography was 180 mm×240 mm, and that for PCM was 350 mm×430 mm. The photostimulable phosphor plate was scanned by an image reader with a sampling rate of 0.04375 mm in the CR unit. Therefore, the effective sampling rate at 1.75 times magnification for PCM was 0.025 mm.

PCM and conventional mammography were conducted under the same exposure conditions. Although conventional mammography uses a bucky to eliminate scattered X-rays, PCM can eliminate scattered X-rays without using a bucky through an air gap effect by creating enough distance between the object and detector. The amount of X-ray dose reduction is approximately the same between that of the conventional imaging with a bucky and PCM with the air gap effect. As a result, the incident dose to the detector is the same for both conventional mammography using a bucky and PCM magnified by a factor of 1.75 without a bucky. Therefore, in clinical practice, the exposure conditions for conventional mammography and PCM are considered to be the same.

3.2 Creation of X-ray images

In the present experiment, the exposure conditions were different for conventional imaging and phase imaging. The reason was that no bucky was used for conventional imaging, as the X-rays scattered after passing through the phantom were negligible. To equalize the incident dose to the detector for both conventional imaging and phase imaging, the exposure conditions for conventional imaging were set at 28 kV and 5 mAs, while those for phase imaging were set at 28 kV and 16 mAs.

Data analysis was conducted after transferring the raw digital image data of the imaged phantom to a personal computer (Dell Inspiron 5100, DELL, TX, U.S.A.), and the data were then post-processed.

3.3 Formation of processed images

Unsharp masking and Laplacian filtering were conducted on conventional images of three acrylic fibers with diameters of 3.0 mm, 5.0 mm, and 7.0 mm, as shown in Figs.3(a)-(c). The parameters for unsharp masking included the mask size and weighting factor (WF). Images processed by unsharp masking were produced with a total of 200 imaging processes based on the combination of 10 mask sizes ranging from 3×3 to 21×21 and 20 different weighting factors ranging from 0.1 to 10. The parameters for Laplacian filtering also consisted of the mask size and weighting factor. Images processed by Laplacian filtering were formed using a total of 128 imaging processes based on the combination of four mask sizes (3×3, 5×5, 7×7, 9×9) and 32 different weighting factors ranging from 0.01 to 10.

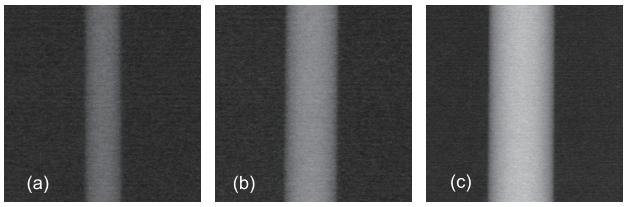

Fig.3 Images of acrylic fiber phantoms used in our experiment. These images were obtained by conventional imaging for acrylic fibers (a) 3.0 mm, (b) 5.0 mm, and (c) 7.0 mm in diameter.

3.4 Method of determining image processing parameters

Profile curves were produced for phase images, conventional images, and images processed by unsharp masking/Laplacian filtering of acrylic fibers. The acrylic fibers were oriented in the longitudinal direction, and each final profile curve was formed by averaging 100 different vertical profile curves from the same image. Fig.4(a) shows the profile curves of phase images and images processed by unsharp masking. The effective sampling pitch for phase imaging on the imaged surface was 0.025 mm (0.04375 mm/1.75 times magnification), while the effective sampling pitch of the conventional and images processed by unsharp masking was 0.04375 mm. In order to equalize the sampling pitches, three-dimensional spline interpolation was done on the profile curves of conventional and images processed by unsharp masking so that the data could be sampled at 0.025 mm intervals. Fig.4(b) shows a zoomed-in view of the profile curve at the edge of the acrylic fibers. To investigate how well the profile curves of the phase image and image processed by unsharp masking agree, regions of

interest (ROIs) were set and the data in the ROIs were compared. The ROIs included a total of 50 data points (0.025 ×50=1.25 mm) centered on the peak at the edge of phase image, with 25 points on each side. The root-mean-square error (RMSE) was calculated at a given mask size by changing the weighting factor based on the profile curves of the image processed by unsharp masking and phase images (true value) shown in Fig.4(c). Next, optimal parameters were defined for each mask size as the combination of weighting factors that yielded the minimum RMSE shown in Fig.4(d).

3.5 Comparison between phase images and post-processed images

Using images of the acrylic phantoms (diameters of screws and spheres: 3.0 mm Φ, 5.0 mm Φ, 7.0 mm Φ, and 9.0 mm Φ), we compared phase image, conventional image, and images processed by unsharp masking/Laplacian filtering with optimal image processing parameters.

3.6 Frequency analyses of phase images and post-processed images

We performed frequency analyses of the phase image, conventional image, and images processed by unsharp masking/Laplacian filtering. Two-dimensional (2D) Fourier transformation was done on the phase image, conventional image, and images processed by unsharp masking/Laplacian filtering with acrylic phantoms (diameters of screws and spheres: 3.0 mm Φ, 5.0 mm Φ, 7.0 mm Φ, and 9.0 mm Φ), and spatial frequency images were obtained.

Band-pass filtering (band width: 1.0 cycle/mm, moved at 1.0 cycle intervals) was performed in the frequency range of 0 to 10 cycles/mm on these spatial frequency images, and then the data were changed back into real-space images by the inverse 2D Fourier transformation. Images from the different subdivided frequency bands were visually evaluated.

4. RESULTS AND DISCUSSION

4.1 Image processing parameters

Figs.5(a) and 5(b) show profile curves of the edges of the acrylic fibers with three different diameters obtained by conventional imaging and phase imaging, respectively. The horizontal axes of these graphs are defined as the distance in the object plane. With conventional imaging, the edge of the acrylic fiber was unclear due to a blurring effect, as shown in Fig.5(a). The acrylic fiber 3.0 mm in diameter had less contrast for the imaged object, resulting in a relatively mild profile curve slope compared with that for fibers 5.0 mm or 7.0 mm in diameter. On the other hand, with phase imaging (Fig.5(b)), the edges of the acrylic fibers were clearly seen because of the edge-enhancement resulting from X-rays refracted in the periphery of the acrylic fibers. Furthermore,

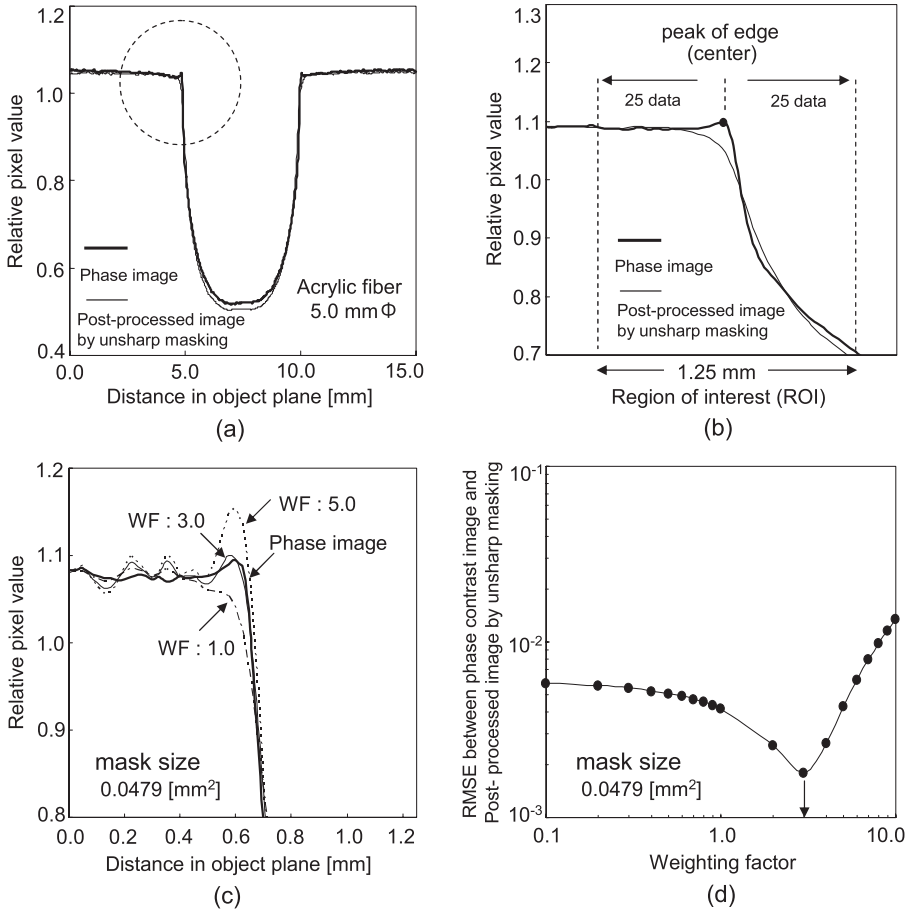

Fig.4 Relation between the relative pixel value and distance in the object plane measured to determine the optimal imaging parameters. (a) Profile curves of acrylic fiber (5 mm Φ) from the image processed by unsharp masking and phase image. The dotted circle shows the ROI. (b) Chosen ROI. (c) Profile curves of the image processed by unsharp masking (mask size: 0.0479 mm²; weighting factor [WF]: 1.0, 3.0, and 5.0) and phase image in the ROI. (d) RMSE between the phase image and image processed by unsharp masking in the ROI.

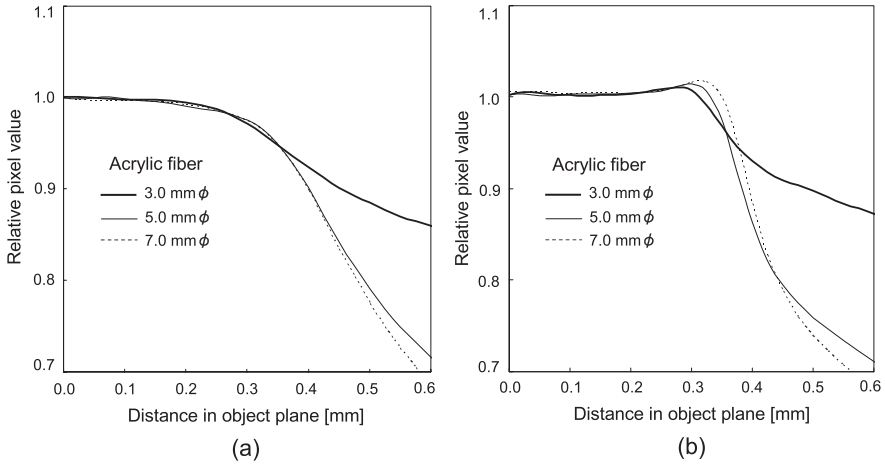

Fig.5 Profile curves of acrylic fibers with three diameters. (a) Conventional image and (b) phase image.

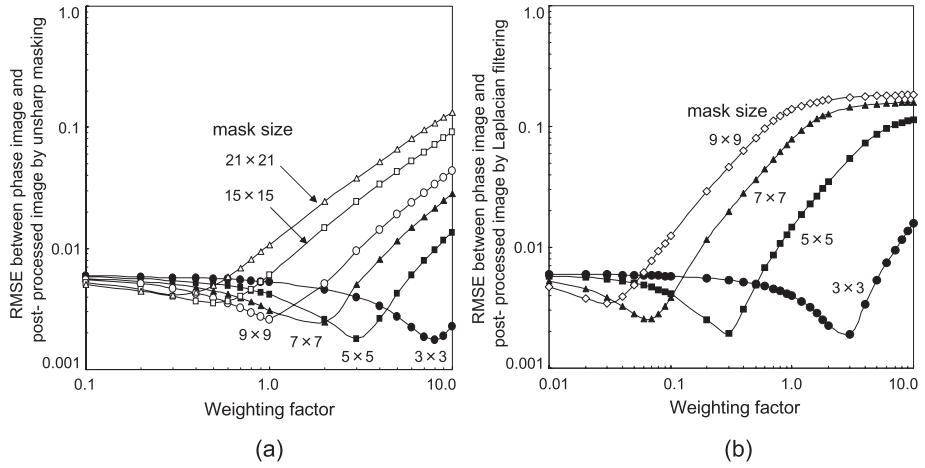

Fig.6 RMSE between phase image and image processed by unsharp masking/Laplacian filtering. An appropriate weighting factor for each mask size was determined for (a) image processed by unsharp masking and (b) image processed by Laplacian filtering. The diameter of the acrylic fiber phantom is 5.0 mm.

the edge-enhancement for larger acrylic fiber diameters was more notable than that for smaller ones, resulting in a steep slope of the profile curves in the peripheral regions.

The aim of our study was to perform sharpness processing on the conventional images shown in Fig.5(a) to produce edge-enhancement effect similar to the phase images shown in Fig.5(b). Figs.6(a) and 6(b) show the RMSE between phase images and post-processed images of the acrylic fiber (5.0 mm in diameter) with unsharp masking and Laplacian filtering, respectively. Optimal imaging parameters were determined by obtaining weighting factors that yield the minimum RMSE for various mask sizes. Based on these graphs, Table 1 shows the optimal processing parameters for three different acrylic fibers for (a) unsharp masking and (b) Laplacian filtering. The relationship between the mask size and weighting factor suggests that a combination of a small mask size and large weighting factor or a large mask size and small weighting factor result in edge-enhanced images similar to the phase images for both unsharp masking and Laplacian filtering. In addition, it was found that (1) the larger the mask size, the larger the RMSE tended to be, and (2) the larger the imaged object, the larger the weighting factor tended to be.

Unsharp masking response functions for four sets of image processing parameters (3×3, 5×5, 7×7, and 9×9), shown in Table 1, with small RMSEs for the acrylic fiber of 5.0 mm in diameter are presented in Fig.7. The unsharp masking response function in the spatial frequency region, $Rs_{\mathrm{um}}(u)$, was calculated according to the following equation [26]:

$$Rs_{\mathrm{um}}(u) = 1 + k\left[1 - \frac{\sin(\pi u N)}{\pi u N}\right], \tag{8}$$

where u is the spatial frequency number, N is the mask size ($n \times$pixel size), and k is the weighting factor. When the mask width is reduced, the enhanced frequency peak shifts toward higher frequencies: the peak of the response function is at 3.5 cycles/mm for a mask width of 9×9 (0.394 mm), 4.5 cycles/mm for 7×7 (0.306 mm), 6.5 cycles/mm for 5×5 (0.219 mm), and 11.0 cycles/mm for 3×3 (0.131 mm). To obtain edge-enhanced conventional images similar to phase images, a combination of a small mask width and a large weighting factor is found to result in high-frequency-enhanced processing. Figs.8(a)-(c) and 8(d)-(f) show profile curves of three acrylic fibers (ROIs of Fig.4(a)) processed by unsharp masking and Laplacian filtering, respectively, using four sets of image processing parameters (3×3, 5×5, 7×7, and 9×9) with small RMSEs shown in Table 1. Fig.8(a) shows the profile curves of edge-enhanced images of acrylic fibers of 3.0 mm diameter post-processed with unsharp masking using four sets of image parameters. However, the edge-enhancement of the images

Table 1 Combinations of mask size and weighing factor as image processing parameters for (a) unsharp masking and (b) Laplacian filtering necessary to obtain edge enhancement in conventional images equivalent to that in phase imaging. RMSE: root mean square error.

(a) Unsharp masking

Mask size [pixels]	Weighting factor (RMSE value)		
	3.0 mmϕfiber	5.0 mmϕfiber	7.0 mmϕfiber
3×3	8 (0.00110)	8 (0.00175)	10 (0.00104)
5×5	3 (0.00112)	3 (0.00178)	4 (0.00169)
7×7	1 (0.00132)	2 (0.00244)	2 (0.00209)
9×9	0.9 (0.00133)	1 (0.00261)	1 (0.00304)
11×11	0.6 (0.00144)	0.8 (0.00295)	0.9 (0.00304)
13×13	0.5 (0.00155)	0.6 (0.00330)	0.7 (0.00370)
15×15	0.4 (0.00163)	0.5 (0.00358)	0.5 (0.00408)
17×17	0.3 (0.00169)	0.4 (0.00380)	0.4 (0.00439)
19×19	0.2 (0.00176)	0.4 (0.00403)	0.4 (0.00458)
21×21	0.2 (0.00179)	0.3 (0.00412)	0.3 (0.00478)

(b) Laplacian filtering

Mask size [pixels]	Weighting factor (RMSE value)		
	3.0 mmϕfiber	5.0 mmϕfiber	7.0 mmϕfiber
3×3	2 (0.00119)	3 (0.00190)	3 (0.00110)
5×5	0.2 (0.00119)	0.3 (0.00195)	0.3 (0.00183)
7×7	0.05 (0.00129)	0.06 (0.00254)	0.07 (0.00267)
9×9	0.02 (0.00152)	0.02 (0.00341)	0.03 (0.00383)

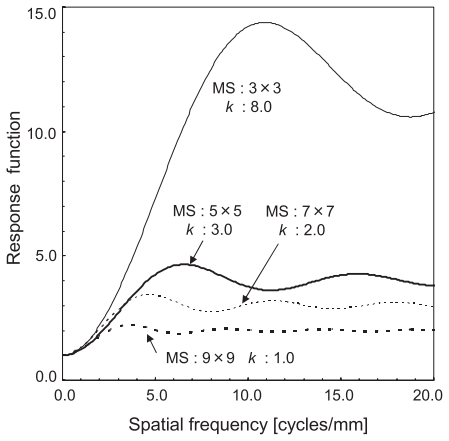

Fig.7 Response functions of unsharp masking response functions for 4 sets of processing parameters with a pixel size of 0.04375 mm. *MS* is mask size and *k* is the weighting factor.

processed by unsharp masking was not as sharp as that of the phase image. The profile curve of the raw image (conventional image) is smooth, because the high-frequency component that delineates the edge of the acrylic fiber was lost. Therefore, no clear difference is seen among the images edge-enhanced with post-processing using the four sets of parameters. This phenomenon is also seen for Laplacian filtering, as shown in Fig.8(d). In Figs.8(b) and (c), which show the profile curves of 5.0 mm and 7.0 mm acrylic fibers, respectively, the profile curves of the images processed by unsharp masking indicate that image processing using a small mask size enables us to obtain sharply edge-enhanced images with a narrow edge. When the peak position of the edge-enhanced images was in the periphery of the acrylic fibers, the margin of the phantom was clearly shown.

When we attempt to obtain images with a similar degree of edge-enhancement using a smaller mask size, the profile curves show large deviations from a smooth curve, because a large weighting factor is necessary for a small mask size, compared with that for a large mask size. Conversely, in the case of a large mask size, the deviation in the profile curve is small, because the weighting factor can be small. These results reflect differences due to the location of the enhanced frequency peak, as shown in Fig.7.

In the present study, we investigated methods to obtain edge-enhanced conventional images with an edge-enhancement effect similar to that of phase imaging. We determined the optimal image processing parameters based on the combination of weighting factor and mask size that yielded the minimum RMSE between the profile curves from images processed by unsharp masking/Laplacian filtering and phase images using three different acrylic fibers. Our experiment showed that the mask size yielding the minimum RMSE was 3×3 for both unsharp masking and Laplacian filtering. For unsharp masking, the optimal processing parameters were defined to be a mask size of 3×3 and a weighting factor of 8.0, because the RMSE had a minimum value at a weighting factor of 8.0 for fiber sizes of 3.0 mm and 5.0 mm. Similarly, for Laplacian filtering, the optimal processing parameters were defined to be a mask size of 3×3 and a weighting factor of 3.0, as the RMSE had a minimum value at a weighting factor of 3.0 for fiber sizes of 5.0 mm and 7.0 mm.

4.2 Comparison between phase images and post-processed images

Figs.9(a) and 9(b) show the conventional image and phase image of the acrylic phantoms (spheres and screw), respectively. Figs.9(c) and (d) show images post-processed by unsharp masking (mask size: 3×3; weighting factor: 8.0) and by Laplacian filtering (mask size: 3×3; weighting factor: 3.0), respectively. The optimal parameters were calculated based on the image of the acrylic fiber 5.0 mm in diameter. The edge of the acrylic sphere phantom of the same diameter

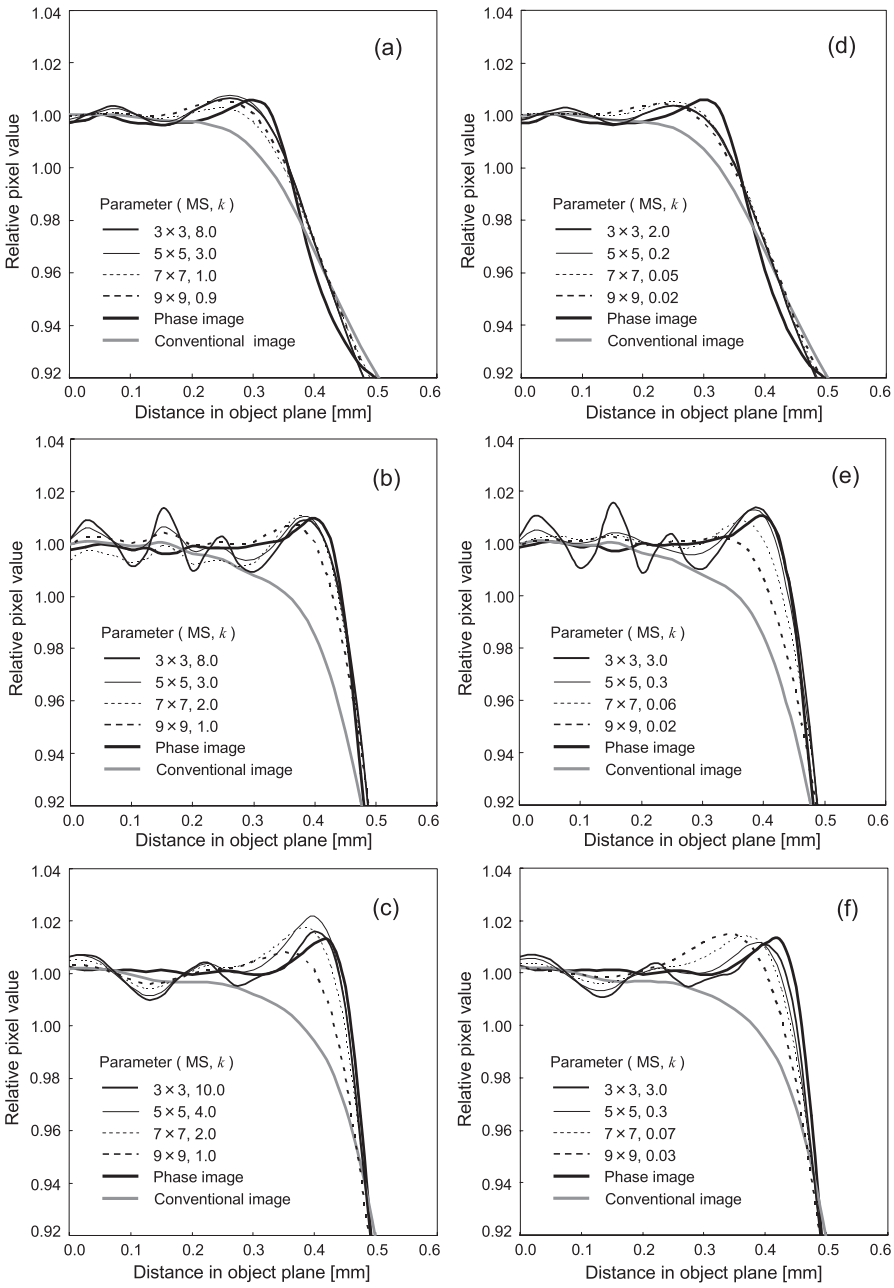

Fig.8 Relation between the relative pixel value and distance in the object plane. Profile curves for four different combinations of *MS* and *k* for image processed by unsharp masking for acrylic fiber phantoms (a) 3.0 mm, (b) 5.0 mm, and (c) 7.0 mm in diameter and for image processed by Laplacian filtering for acrylic fiber phantoms (d) 3.0 mm, (e) 5.0 mm, and (f) 7.0 mm in diameter, along with those from the phase image and conventional image. *MS* is mask size and *k* is the weighting factor.

(5.0 mm) was clearer on images processed by unsharp masking/Laplacian filtering than on conventional images. A similar tendency was found on images of acrylic phantom of different sizes (spheres and screw). However, more noise was seen on images processed by unsharp masking/Laplacian filtering than on phase images, which degraded the image quality.

4.3 Frequency analyses of phase images and post-processed images

As described in the above section 4.2, edge-enhancement of the images processed by unsharp masking/Laplacian filtering was not as good as that of the phase images. We investigated the cause of this by analyzing the frequencies of the conventional image, phase image and images processed by unsharp masking/Laplacian filtering.

Fig.10 shows the acrylic screw phantom images separated into 5 frequency regions (ranging from 0.0 to 5.0 cycles/mm) with a band width of 1.0 cycle/mm. The contrast of phantom images had already been determined for the conventional image, image processed by unsharp masking, and phase image in the frequency band region of less than 1.0 cycle/mm. For frequency bands higher than 1.0 cycle/mm, the edge portion of the phantom image was produced. In the frequency band of 1.0 to 2.0 cycles/mm, no significant difference was found among the conventional image, image processed by unsharp masking, and phase image. In the frequency band of 2.0 to 3.0 cycles/mm, signal intensity of the phantom on the conventional image was lower than that of image processed by unsharp masking or phase image. The image processed by unsharp masking had high signal intensity due to edge-enhancement

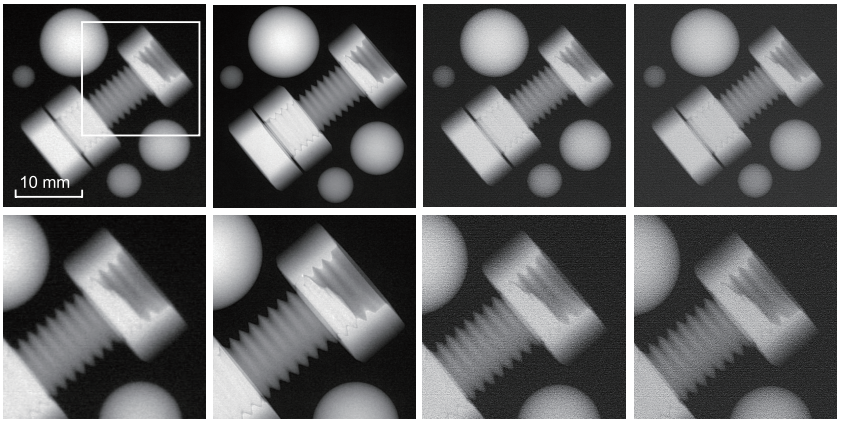

Fig.9 Acrylic phantom images used for the visual assessment. (a) Conventional image, (b) phase image, (c) image processed by unsharp masking (mask size : 3×3 ; k : 8.0 ; pixel size : 0.04375 mm), and (d) image processed by Laplacian filtering (mask size : 3×3 ; k : 3.0 ; pixel size : 0.04375 mm). The images at the bottom are zoomed-in views of the region surrounded by the white square in the top images.

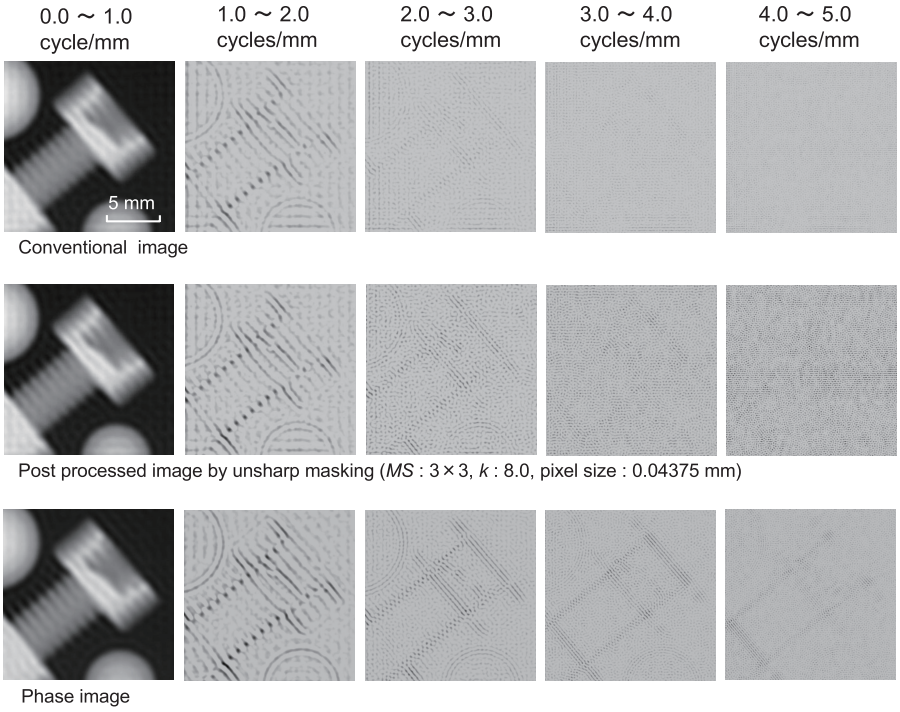

Fig.10 Images of the acrylic phantom (Fig.9) separated in each frequency segment obtained from the conventional image, image processed by unsharp masking, and phase image, all of which are processed with the band-pass filter.

processing ; however, it also had notably increased noise. In contrast, the phase image had very small noise in spite of having high signal intensity. In the high frequency bands of 3.0 to 4.0 cycles/mm and 4.0 to 5.0 cycles/mm, though signal components were not detected on the conventional image, high signal components existed on the phase image. The signal components were not detected on the post-processed image, although high frequency components were enhanced by unsharp-masking. This is considered because the signal intensity of the high frequency band on the conventional images are so small that the signal components are hidden in the noise. Thus, new signals in the high frequency band cannot be obtained by image processing of conventional images.

5. CONCLUSION

The aim of the present study was to investigate whether we could improve the quality of conventional images through sharpening to a degree where it is equivalent to that of phase images. For such sharpening, we used unsharp masking, which has been generally used for medical imaging, and Laplacian filtering, which has been generally used in the engineering field.

Our results suggest that edge-enhanced images with a quality similar to that of phase images are obtainable by sharpening of conventional images with a small mask size ; however, the edge clarity of the images processed by unsharp masking/Laplacian filtering is less than that of the phase images. Moreover, the image quality of the images processed by unsharp masking/Laplacian filtering is far lower than that

of the phase images, due to the increased noise resulting from image processing.

6. Acknowledgements :

The authors appreciate fruitful discussion with Dr. Chika Honda, Mr. Hiromu Ohara of Konica Minolta Medical and Graphic, Inc. We also thank Prof. Kiyoshi Murata of Shiga University of Medical Science for their permission to publish this work.

7. References :

[1] R. E. Johnston, D. Washburn, E. Pisano, C. Burns, et al. : Mammographic phantom studies with synchrotron radiation, Radiology, 200, 659-663, 1996.

[2] Yagi N, Suzuki Y, and Umetani K : Refraction-enhanced x-ray imaging of mouse lung using synchrotron radiation source, Med. Phys., 26, 2190-2193, 1999.

[3] S. W. Wilkins, T. E. Gureyev, D. Gao, et al. : Phase-contrast imaging using polychromatic hand x rays, Nature, 384, 335-338, 1996.

[4] A. Pogany, D. Gao, S. Wilkins : Contrast and resolution in imaging with a microfocus x-ray souce, Rev. Sci. Instrum., 68, 2774-2782, 1997.

[5] R. Fitzgerald : Phase-sensitive x-ray imaging, Phys. Today, 53, 23-26, 2000.

[6] P. Monnin, S. Bulling, J. Hoszowska, et al. : Quantitative characterization of edge enhancement in phase contrast x-ray imaging, Med. Phys., 31, 1372-1383, 2004.

[7] C. J. Kotre and I. P. Birch : Phase contrast enhancement of x-ray mammography -A design study-, Phys. Med. Biol., 44, 2853-2866, 1999.

[8] Ishisaka A, Ohara H, and Honda C : A new method of analyzing edge effect in phase contrast imaging with incoherent x-rays, Optical Review 7, 566-572, 2000.

[9] Honda C, Ohara H, and Ishisaka A : X-ray imaging using a x-ray tube with a small focal spot, Jpn. J. Med. Phys., 22, 21-28, 2002.（in Japanese）

[10] X. Wu, H. Liu : Clinical implementation of x-ray phase-contrast imaging–Theoretical foundations and design considerations–, Med. Phys., 30, 2169-2179, 2003.

[11] X. Wu and H. Liu : A new theory of phase –contrast x-ray imaging based on Wigner distributions, Med. Phys., 31, 2378-2384, 2004.

[12] E. F. Donnelly, R. R. Price, and D. R. Pickens : Dual focal-spot imaging for phase extraction in phase-contrast radiography, Med. Phys., 30, 2292-2296, 2003.

[13] Tohyama K, Katafuchi T, Matsuo S, et al. : Application of phase contrast imaging to mammography, Jpn. J. Radiol. Technol., 61, 245-252, 2005.（in Japanese）

[14] Matsuo S, Katafuchi T, Tohyama K, et al. : Evaluation of edge effect due to phase contrast imaging for mammography, Med. Phys., 32, 2690-2697, 2005.

[15] Ohara H, Honda C, and Ishisaka A : Digital phase imaging using an X-ray tube with a small focal spot, Photographic Science and Technology, 65, 501-505, 2002.（in Japanese）

[16] Honda C : Fundamental technical concept of digital phase contrast mammography, Jpn. J. Medical Imaging and Information Sciences, 21, 230-238, 2004.（in Japanese）

[17] Tanaka T, Honda C, Matsuo S, et al. : The first trial of phase contrast imaging for digital full-field mammography using a practical molybdenum x-ray tube, Investigative Radiology, 40, 385-396, 2005.

[18] Matsuo S, Morishita J, Fujita H, et al. : Evaluation of edge enhancement in a digital phase contrast imaging, Jpn. J. Medical Imaging and Information Sciences, 23, 120-123, 2006.（in Japanese）

[19] Honda C, Ohara H, and Gido T : Image quality of phase contrast mammography, Digital Mammography, R. Zwiggelaar（Ed.）, Springer Lectures Notes in Computer Science（LNCS）series, LNCS4046, Springer, 281-288, 2006.

[20] Honda C, and Ohara H : Advantage of magnification in digital-phase contrast mammography using a practical X-ray tube, European Journal Radiology, 68S, 69-72, 2008.

[21] Matsuo S, Fujita H, Morishita J, et al. : Fundamentals of phase contrast mammography, Radiological Society of North America, 710, 2007.

[22] Matsuo S, Fujita H, Morishita J, et al. : Evaluation of a phase contrast imaging with digital mammography, Digital Mammography, E.A.Krupinski（Ed.）, Springer Lectures Notes in Computer Science（LNCS）series, LNCS5116, Springer, 130-136, 2008.

[23] Yamazaki A, Ichikawa K, and Kodera Y : nvestigation of physical image characteristics and phenomenon of edge enhancement by phase contrast using equipment typical for mammography, Med. Phys., 35, 5134-5150, 2008.

[24] Matsuo S, Fujita H, Morishita J, et al. : Introducing a novel image quality measure for digital phase-contrast-image evaluation, Digital Mammography, J.Marti, A. Oliver, J.Freixenet, and R.Marti（Eds.）, Springer Lectures Notes in Computer Science（LNCS）series, LNCS6136, Springer, 137-144, 2010.

[25] R. C. Gonzalez and R. E. Woods, Digital Image Processing 3rd Ed., Pearson Education Inc., 160-165, New Jersey, USA, 2008.

[26] L. N. Loo, K. Doi, and C. E. Metz : Investigation of basic imaging properties in digital radiography. 4. Effect of unsharp masking on the detectability of simple patterns, Med. Phys., 12, 209-214, 1985.